Direct Experimental Evidence of Back-Surface Ion Acceleration from Laser-Irradiated Gold Foils

Matthew Allen,[1,2,*] Pravesh K. Patel,[2] Andrew Mackinnon,[2] Dwight Price,[2] Scott Wilks,[2] and Edward Morse[1]

[1]*Department of Nuclear Engineering, University of California, Berkeley, California 94720, USA*

[2]*Lawrence Livermore National Laboratory, Livermore, California 94550, USA*

(Received 17 February 2004; published 29 December 2004)

Au foils were irradiated with a 100-TW, 100-fs laser at intensities greater than 10^{20} W/cm^2 producing proton beams with a total yield of $\sim 10^{11}$ and maximum proton energy of >9 MeV. Removing contamination from the back surface of Au foils with an Ar-ion sputter gun reduced the total yield of accelerated protons to less than 1% of the yield observed without removing contamination. Removing contamination from the front surface (laser-interaction side) of the target had no observable effect on the proton beam. We present a one-dimensional particle-in-cell simulation that models the experiment. Both experimental and simulation results are consistent with the back-surface acceleration mechanism described in the text.

DOI: 10.1103/PhysRevLett.93.265004 PACS numbers: 52.38.Ph, 29.27.Fh, 52.65.Rr, 52.70.Nc

The discovery that ultraintense laser pulses ($I > 10^{18}$ W/cm^2) can produce short pulse, well collimated, high energy proton beams [1–4] has renewed interest in the fundamental mechanisms that govern particle acceleration from laser-solid interactions (cf. Ref. [5], and references therein). Experiments have shown that protons present as hydrocarbon contaminants on laser targets can be accelerated up to energies >50 MeV [1]. Well diagnosed and controllable proton beams will have many applications: fast ignition [6], production of medical isotopes [7], and as a high-resolution radiography tool for diagnosing opaque materials and plasmas [8,9].

Different theoretical models that explain the observed results have been proposed. One model describes a front-surface acceleration mechanism based on the ponderomotive potential of the laser pulse [10]. At high intensities ($I > 10^{18}$ W/cm^2), the quiver energy of an electron oscillating in the electric field of the laser pulse exceeds the electron rest mass, requiring the consideration of relativistic effects. The relativistically correct ponderomotive potential is given by

$$U_p = \left(\left[1 + \frac{I\lambda^2}{1.3 \times 10^{18}}\right]^{1/2} - 1\right) m_0 c^2, \qquad (1)$$

where $I\lambda^2$ is the irradiance in W μm^2/cm^2 and m_0c^2 is the electron rest mass [11]. Recent experiments that consider this ponderomotive potential sufficiently strong to accelerate protons from the front surface of the target to energies up to tens of MeV have been reported [12–14].

Another model, known as target normal sheath acceleration (TNSA) proposed by Hatchett *et al.* and Wilks *et al.* in Refs. [15,16] (and references therein), reintroduces a back-surface electrostatic sheath mechanism in the short-pulse, high-temperature plasma regime. According to the TNSA model, relativistic hot electrons created at the laser-solid interaction penetrate the foil where a few escape to infinity. The remaining hot electrons are retained by the target potential and establish an electrostatic sheath on the back surface of the target. The electric field associated with this sheath has the form

$$\vec{E} \approx \frac{k_B T_e}{e\lambda_D}, \qquad (2)$$

where k_BT_e is the electron temperature, e is the electron charge, and $\lambda_D = (\varepsilon_0 k_B T_e / e^2 n_e)^{1/2}$ is the standard Debye length. Typical electron temperatures and scale lengths of $k_BT_e \sim 2$ MeV and $\lambda_D \sim 2$ μm for ultraintense laser-plasma interactions can result in an electric field on the back surface of the target of $\vec{E} > 10^{12}$ V/m. At this field strength, contaminants on the back surface of the target are field ionized and accelerated to high energies over the short scale length of the electric field. Protons are preferentially accelerated due to their high charge-to-mass ratio and subsequently shield heavier ions from the electric field. Recent experiments that consider the TNSA model capable of accelerating protons up to tens of MeV have been reported [1,17–19].

Selectively removing contaminants from either the front or back surface of a laser target, and subsequently observing the producible proton beam, has been proposed as a means of determining the dominant physical model within a fixed set of experimental parameters. Mackinnon *et al.* used a secondary laser to create a 100-μm scale length plasma on the back of the foil, which reduced the maximum proton energy to <5 MeV and greatly reduced the proton yield [19,20]. However, using a long-pulse laser to irradiate the back surface is a rather large perturbation of the foil, and it is difficult to isolate the effect of removing the contaminants from the possible laser-plasma interactions caused by the secondary laser pulse. Hegelich *et al.* showed that resistively heating targets reduced the amount of contamination and allowed for the acceleration of heavier ions from the bulk material of the target up to energies >5 MeV/nucleon [17]. Resistively heating, however, re-

moves contaminants from both sides of a laser target and does not allow for the direct comparison of front-surface to back-surface proton acceleration.

In this Letter, we present conclusive evidence that >99% of MeV-energy protons observed from the interaction of an ultraintense laser pulse with a thin metallic foil originate from hydrogenous contaminants on the back surface of the target. Using an argon-ion sputter gun, contaminants from one side of the laser target were selectively removed without affecting the other side. Irradiating a 15-μm-thick gold foil with an ultraintense laser pulse produced a proton beam with a total yield $>10^{11}$ protons and maximum proton energy of >9 MeV. Removing contaminants from the front surface (laser-interaction side) of the laser target produced a proton beam with similar yield and maximum proton energy. However, when contaminants were removed from the back surface of the laser target, the total proton yield was reduced to less than 1% of the contaminants present case, and the maximum proton energy was limited to less than 4 MeV. Our results unambiguously show the *back* surface TNSA model to be the dominant acceleration mechanism for protons with energies >3 MeV.

Experiments were preformed at the JanUSP laser facility of the Lawrence Livermore National Laboratory (LLNL). JanUSP is a Ti:sapphire laser operating at a wavelength of 0.8 μm and delivering 10 J of energy in a pulse duration of 100 fs [21]. The pulse was focused onto the target at 22° by an $f/2$ off-axis parabola to a focal spot with diameter 3–5 μm at the full width at half maximum (FWHM). This gave an irradiance on target of $I\lambda^2 > 10^{20}$ W μm^2/cm^2. The amplified spontaneous emission (ASE) prepulse level was measured to be no greater than 10^{-8} of the main pulse intensity. A stack of radiochromic film (RCF) was placed 26 mm behind and normal to the back surface of the laser target. RCF is a dosimetry film that measures radiation dose or deposited energy by turning blue when exposed to ionizing radiation. An 18-μm-thick Al blast shield protected the film from target debris. Two types of RCF were used, GARCHROMIC® HD-810 and HS [22]. The former, with a thin (6.5 μm) dye layer on top of a 100-μm-thick polyester substrate, is useful in detecting low energy protons. The latter, HS, has a 40 μm dye layer sandwiched *between* 100-μm-thick layers of polyester, which increases sensitivity but prohibits the detection of protons with energies <5 MeV. The deposited dose as a function of optical density for the RCF was determined by irradiating the film with a cobalt-60 source of known activity [1]. Previous experiments at multiple institutions—through a combination of RCF, CR-39, and nuclear activation—have demonstrated that the observed signal on the RCF is the result of proton energy deposition [1,4,13].

Targets used in the experiment were all 15-μm-thick gold foils with optical quality surface roughness. The contamination present on the targets was characterized by x-ray photoemission spectroscopy, which showed a 12-Å-thick layer consisting of 27% gold, 60.5% hydrocarbons (CH_2), and 12.2% water vapor (H_2O). We can calculate a density for this surface layer by summing the fractional densities of each component $\rho_{\mathrm{av}} = 0.27 \times 19.3 + 0.605 \times 1 + 0.122 \times 1 = 5.938$ g/cm^3. The atom density of hydrogen in the mixture is given by $N = 4(\rho_{\mathrm{av}} N_A / M_{\mathrm{av}})$, where N_A is Avogadro's number and M_{av} is the average molecular mass of the hydrogenous pseudomolecule. The factor of 4 represents the number of hydrogen atoms in the pseudomolecule. Taking $M_A = (0.27 \times 197 + 0.60 \times 14 + 0.122 \times 18) = 63.79$ g, we calculate the hydrogen atom density to be $N = 2.24 \times 10^{23}$ atoms/cm^3. Previous measurements on the JanUSP laser have shown the source size of the proton beam on the back surface of the target to be ~200 μm in diameter [23], which corresponds to a possible volume for the 12 Å hydrogenous surface layer of 3.8×10^{-11} cm^3. The total number of protons p^+_{tot} available to be accelerated by the rear surface electrostatic sheath is then given by the product of the atom density and the volume, which we calculate to be $p^+_{\mathrm{tot}} \sim 8.4 \times 10^{12}$.

A 3 cm CommonWealth argon-ion sputter gun was used to remove surface contaminants. The sputter gun was operated with a beam voltage and beam current of 500 V and 10 mA, respectively. Calibration was performed *in situ* by etching an aluminum surface of optical quality roughness and was found to etch at a rate of ~170 Å/min. The sputter gun could be positioned to etch either the front surface (laser-interaction side) or the back surface of the laser target with the same gun-to-target distance of 11 cm. At this distance, the thermal radiation from the filament inside the sputter gun had no effect had on the temperature of the thin foil. The sputter gun was on continuously during the laser shot. This ensured the target surface under examination was free of contaminants when the laser fired. The vacuum in the experimental chamber was characterized with a residual gas analyzer and found to be predominately water vapor at a pressure of 2×10^{-5} torr. Hydrocarbon residue was present at a lower pressure of $\sim 10^{-7}$ torr.

The detected proton beam from irradiating a gold target at an energy of 6.94 J is shown in Fig. 1(a). The data show a well collimated, smooth 2D spatial image of the proton beam up to a maximum energy of >9 MeV, which was a typical and highly repeatable result for targets of the same thickness at comparable laser energies. Figure 1(b) shows the proton beam from a shot with 8.41 J on a target in which the front surface was etched for 2.6 min. Similar to part (a), the data show a well collimated proton beam up to a maximum energy of >9 MeV. Etching the back surface of the laser target, however, has a dramatic effect, as shown in Fig. 1(c). This shot had a comparable laser energy of 7.67 J but was etched on the *back* surface for 4.0 min.

Etching the back surface of the target greatly reduced the proton beam number and maximum energy to less than 4 MeV, detectable only on the first two layers of the RCF. Reduction of the proton beam was highly reproducible on many shots with back surface etch times of ~2 min (corresponding to >300 Å of material).

At energies greater than 5 MeV, the proton beam can be fit to a Maxwellian distribution of the form $N(E) = N_0[2/\sqrt{\pi}(kT)^{3/2}]\sqrt{E}\, e^{-E/kT}$, where N_0 represents the total proton number and kT is the temperature of the distribution in mega-electron-volts. For an analytic description of the proton spectrum, please refer to Ref. [24]. The energy deposited in each active dye layer of RCF is plotted with the measured dose of the experimental data obtained from the optical density. The proton number (N_0) and temperature (kT) are then adjusted interactively to achieve the best fit with the data. The analysis of the data shown in Fig. 1 is presented quantitatively in Fig. 2. Above 5 MeV, the shot without etching and the shot in which the front surface was etched both produced a good quality beam with proton yields of $(1.5–2.5) \times 10^{11}$ and temperature $kT = 1.5$ MeV. Etching the back surface of the target produced no measurable proton beam (at $E > 5$ MeV) above background levels. This corresponds to a maximum possible yield of $\sim 10^9$ for our experimental parameters.

To gain insight into the ion acceleration mechanisms present near the target surfaces, we performed 1D particle-in-cell (PIC) computer simulations [25]. Given the extremely laminar quality and ultralow emittance of the proton beam [26], we perceive 1D simulations sufficient to reasonably model our experiment. In these simulations, the solid is approximated by a 15-μm slab of plasma with the following characteristics: electron density ramps up from 0 to 60 n_{cr} over 1.4 μm and is equal to 60 n_{cr} for 15 μm, with an abrupt falloff to 0 n_{cr} over 8 Å. The slope roughly models the preformed plasma created by the prepulse and ASE that exist in front of the laser. The short laser pulse itself (peak $I = 8 \times 10^{19}$ W/cm^2, pulse length 100 fs FWHM) is incident on the sloped side. A schematic of the density profile is shown in Fig. 3(a). The bulk of the ions were taken to have a charge-to-mass ratio of 0.005 583 times that of the protons in order to model heavy gold ions at an ionization of 11 + . This level of ionization is predicted by the field ionized barrier suppression model for the fifth electron of the gold atom with an ionization potential of 61.1 eV at field strengths $>10^{12}$ V/m [17,27]. There is a thin sheet of protons on the front surface of the target raising to 3 n_{cr} over a distance of 0.10 μm and an 8-Å-thick layer of protons on the back surface as existed in the experiment. The simulation was run for 500 fs, at which time further acceleration of the protons was not observed.

We can see from Fig. 3(b) that protons from the back surface obtain an energy range 5–14 MeV, which is consistent with the experimental results when the target was not etched or etched only on the front side as seen in Figs. 1(a) and 1(b). The simulation also shows that the heavy gold ions reach a maximum energy of 140 MeV, which is insufficient to penetrate the 18-μm-thick Al blast shield in front of the film pack. Therefore, we cannot attribute any of the energy deposited in the film to the heavy gold ions.

We can also see from Fig. 3(b) that the front-surface protons reach a maximum energy of ~4 MeV, consistent with the laser ponderomotive potential on the front surface of the target. At this energy, it is conceivable that front-surface protons could penetrate the length of the gold target and the aluminum blast shield to deposit their *remaining*

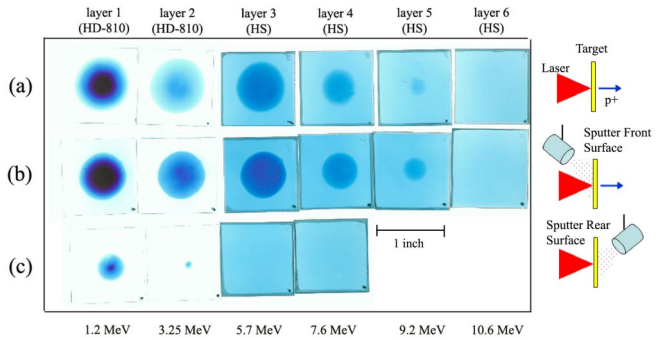

FIG. 1 (color online). Observed proton beam from 15-μm-thick Au targets. The type of film at each layer in the film pack is shown above the data, and the average proton energy at that layer is shown below the data. (a) Laser energy of 6.94 J; no ion etching. (b) Laser energy of 8.41 J; front surface (laser side) of target was etched for 2.6 min. (c) Laser energy of 7.67 J; back surface of target was etched for 4.0 min.

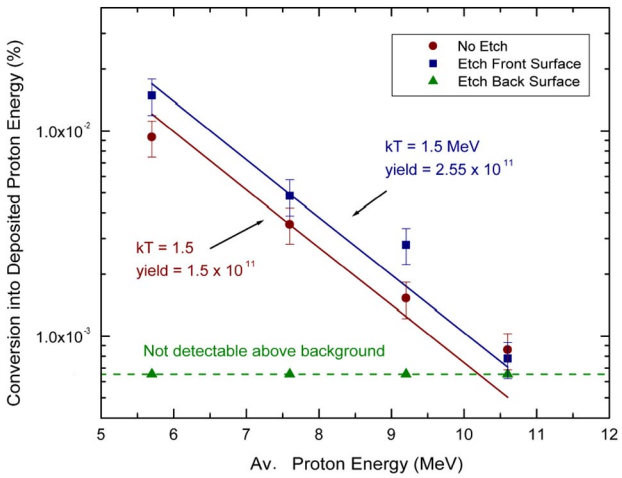

FIG. 2 (color online). Proton spectra from 15-μm-thick Au targets fit to a Maxwellian distribution. Shots that were etched only on the front surface or not etched at all show a temperature of $kT = 1.5$ MeV above proton energies of 5 MeV. Shots that were etched on the back surface produced no measurable proton beam above background levels.

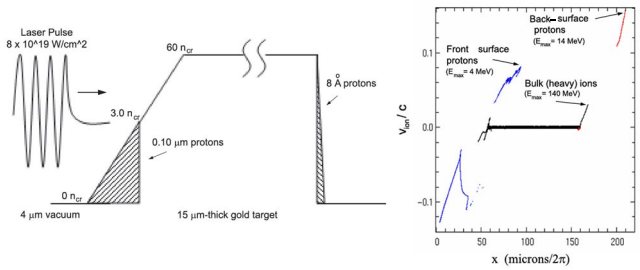

FIG. 3 (color online). (a) Density profiles used in PIC simulation, described in the text. (b) Result of 1D PIC simulation at time $t = 500$ fs. Protons from the back surface of the target obtain energies between 5 and 14 MeV. Front-surface protons reach a maximum energy of 4 MeV. Heavy (gold) ions reach a maximum energy of 140 MeV.

energy (< 3 MeV) in the first one or two layers of thin RCF. Independent PIC simulations by Wilks *et al.* and Pukhov in Refs. [16,28], respectively, have shown that protons accelerated from the front surface have a much larger emittance angle than those accelerated from the back surface. The fact that the bright center spot of Fig. 1(c) is so well collimated and in the same alignment as the proton beams shown in Figs. 1(a) and 1(b) tends to argue against the case for front-surface protons which have a broad spatial distribution. Given that the image on the first two pieces of film in Fig. 1(c) is in the same position as the images of Figs. 1(a) and 1(b), we attribute the signal to protons on the back surface of the target that were not removed by ion sputtering. The generated proton beam was decreased in yield to such an extent that no signal was detectable at energies $E > 5$ MeV.

In conclusion, we have shown that irradiating a thin metallic foil with an ultraintense laser pulse produces a well collimated proton beam with a yield of $(1.5–2.5) \times 10^{11}$ and temperature $kT = 1.5$ MeV with a maximum proton energy >9 MeV. Removing contaminants from the front surface of the laser target with an argon-ion sputter gun had no observable effect on the producible proton beam. However, removing contaminants from the *back* surface of the laser target reduced the proton beam by 2 orders of magnitude to, at most, a yield of $\sim 10^9$ and a maximum proton energy <4 MeV. Based on these observations, we conclude that the majority ($> 99\%$) of high energy protons ($E > 5$ MeV) from the interaction of an ultraintense laser pulse with a thin foil originate on the *back* surface of the foil. Our experimental results are in agreement with PIC simulations showing that back-surface protons reach energies up to 14 MeV, while front-surface protons reach a maximum energy of 4 MeV.

The authors would like to thank Tom Thurman of π-Scientific (www.piscientific.com) for support in refurbishing and customizing our sputter gun and the entire JanUSP support staff for their assistance during the experiment. This work was funded under the auspices of the U.S. Department of Energy by the Lawrence Livermore National Laboratory under Contract No. W-7405-ENF-48.

*Corresponding author.
Electronic address: mallen@nuc.berkeley.edu

[1] R. Snavely *et al.*, Phys. Rev. Lett. **85**, 2945 (2000).
[2] A. Maksimchuk, S. Gu, K. Flippo, D. Umstadter, and V. Bychenkov, Phys. Rev. Lett. **84**, 4108 (2000).
[3] E. Clark *et al.*, Phys. Rev. Lett. **84**, 670 (2000).
[4] M. Roth *et al.*, Phys. Rev. ST Accel. Beams **5**, 061301 (2002).
[5] S. J. Gitomer *et al.*, Phys. Fluids **29**, 2679 (1986).
[6] M. Roth *et al.*, Phys. Rev. Lett. **86**, 436 (2001).
[7] K. Nemoto *et al.*, Appl. Phys. Lett. **78**, 595 (2001).
[8] M. Borghesi *et al.*, Phys. Rev. Lett. **88**, 135002 (2002).
[9] A. J. Mackinnon *et al.*, Appl. Phys. Lett. **82**, 3188 (2003).
[10] S. C. Wilks, W. L. Kruer, M. Tabak, and A. B. Langdon, Phys. Rev. Lett. **69**, 1383 (1992).
[11] W. L. Kruer and S. C. Wilks, *Introduction to Ultra-Intense Laser-Plasma Interactions* (AIP, New York, 1994), p. 16.
[12] E. Clark *et al.*, Phys. Rev. Lett. **85**, 1654 (2000).
[13] M. Zepf *et al.*, Phys. Rev. Lett. **90**, 064801 (2003).
[14] L. O. Silva, M. Marti, J. R. Davies, and R. A. Fonseca, Phys. Rev. Lett. **92**, 015002 (2004).
[15] S. P. Hatchett *et al.*, Phys. Plasmas **7**, 2076 (2000).
[16] S. C. Wilks *et al.*, Phys. Plasmas **8**, 542 (2001).
[17] M. Hegelich *et al.*, Phys. Rev. Lett. **89**, 085002 (2002).
[18] A. J. Mackinnon *et al.*, Phys. Rev. Lett. **88**, 215006 (2002).
[19] A. J. Mackinnon *et al.*, Phys. Rev. Lett. **86**, 1769 (2001).
[20] M. Borghesi *et al.*, Phys. Rev. Lett. **92**, 055003 (2004).
[21] J. D. Bonlie, F. Patterson, D. Price, B. White, and P. Springer, Appl. Phys. B Suppl. **70**, S155 (2000).
[22] ISP, Gafchromic Radiation Dosemitry Media (2003), URL http://www.ispcorp.com/products/dosimetry.
[23] P. K. Patel *et al.*, Phys. Rev. Lett. **91**, 125004 (2003).
[24] P. Mora, Phys. Rev. Lett. **90**, 185002 (2003).
[25] A. B. Langdon and B. F. Lasinski, *Methods in Computational Physics* (Academic, New York, 1976), Vol. 16, pp. 327–366 (description of ZOHAR laser-plasma PIC code).
[26] T. Cowan *et al.*, Phys. Rev. Lett. **92**, 204801 (2004).
[27] J. Scofield (private communication).
[28] A. Pukhov, Phys. Rev. Lett. **86**, 3562 (2001).